

Dependent landmark drift: robust point set registration based on the Gaussian mixture model with a statistical shape model

Osamu Hirose

Faculty of Electrical and Electronic Engineering, Institute of Science and Engineering, Kanazawa University,
Kakuma, Kanazawa, Ishikawa 920-1192, JAPAN.

E-mail: hirose@se.kanazawa-u.ac.jp

Abstract. Point set registration is to find point-by-point correspondences between point sets, each of which characterizes the shape of an object. Due to the assumption of the local preservation of object geometry, prevalent algorithms in the area can often elegantly solve the problems without using geometric information specific to the objects. This means that registration performance can be further improved by using the prior knowledge of object geometry. In this paper, we propose a novel point set registration method using the Gaussian mixture model with prior shape information encoded as a statistical shape model. Our transformation model is defined as the combination of the rigid transformation, the motion coherence, and the statistical shape model. Therefore, the proposed method works effectively if the target point set includes outliers and missing regions, or if it is rotated. The computational cost can be reduced to linear and thereby the method is scalable to large point sets. The effectiveness of the method will be verified through comparisons with existing algorithms using datasets concerning human hands and faces.

Keywords: Point set registration, Gaussian mixture model, statistical shape model, EM algorithm

1 Introduction

Point matching is the problem of finding point-by-point correspondence between point sets where each set characterizes the geometry of an object. Finding such geometrical correspondences between point sets is studied in the fields of image recognition and computer vision. A major class of point matching problems is point set registration—the problem of finding a transformation between two point sets in addition to point-by-point correspondences. Point set registration problems can be roughly classified into two classes according to the transformation models: rigid and non-rigid transformations. A rigid transformation model is defined as a linear map that preserves the relative positions of points in a point set, i.e., scaling, rotation, and translation. The rigid point set registration problem is a relatively simple problem that has been intensively studied [1, 2, 3, 4, 5]. Non-rigid registration is a more complex problem that involves transforming an object’s geometry. Typical transformation models used for point set registration problems are the thin-plate spline functions [6, 7, 8, 9, 10] and the Gaussian functions [11, 12, 13, 14]. These methods are differently classified according to the definitions of the point set registration problem: energy minimization [6, 7, 10], and probabilistic density estimation using a Gaussian mixture model [8, 9, 11, 12, 13, 14].

Crucial to the success of these registration methods is a robustness to outliers, points that are irrelevant to the true geometry of the object. Several approaches have been proposed to deal with outliers, such as statistical analysis for distances between correspondent points [15, 16, 17], soft assignments [7, 18], trimming point sets through iterative random sampling [19], kernel correlation [20], explicit probabilistic modeling of outliers [11, 12, 13, 14], the use of a robust estimator—the L_2E estimator [8] and a scaled Geman–McClure estimator [21]. Another factor crucial to the success of registration methods is the assumption of a smooth displacement field, which forces neighboring points to move coherently. The smoothness of the displacement field is imposed by a regularization technique defined as a penalty term for energy minimization [6, 7, 10] and a penalty term for log-likelihood functions [8, 9, 11, 12, 13, 14]. Due to the assumption of a smooth displacement field, such non-rigid registration algorithms seek to find transformations with sufficient global flexibility while preserving the local topology of a point set.

These methods are universally applicable to general point set registration problems as no prior knowledge, except for that concerning the smoothness of a displacement field, is assumed to the geometry of objects to

be registered. This means that registration performance can be improved by using prior knowledge of object geometry instead of sacrificing applicability. One approach to incorporating such prior information is the use of a kinematic motion for articulated objects, such as the human body [22, 23, 24, 25]. These methods show promising results but cannot be applied to objects with no kinematics. Another approach is the use of partial correspondence across two point sets [26, 27]. These methods also show promising results, but better performance is not expected if partial correspondence is not available. Yet another approach is the use of supervised learning techniques. One candidate of such supervised learning techniques is a statistical shape model [28, 29, 30, 31] that describes the mean shape and statistical variation of geometrical objects. Shape variations represented by statistical shape models are constructed from shape statistics of landmark displacements. Therefore, movements of neighboring landmarks are not assumed to be correlated, and those of distant landmarks are allowed to be dependent on one another. Statistical shape models also do not require any physical models such as object kinematics. Statistical shape models have been widely used as prior shape information for various tasks, such as image registration and image segmentation in the field of computer vision and medical imaging [31, 32, 33]. Typical implementations of these algorithms, however, are not specialized for point set registration problems.

Contributions of this work

In this article, we propose a novel non-rigid point set registration algorithm based on a supervised learning approach that we call dependent landmark drift (DLD). It aims to solve point set registration problems under the conditions whereby (i) complete point-by-point correspondence across multiple point sets are available as training data, and (ii) no partial correspondence across two point sets to be registered, e.g., test data, is available. In the context of statistical shape modeling, the proposed algorithm is a novel optimization algorithm for fitting statistical shape models, where each of two input datasets to be registered is a set of points without additional information such as colors and surface normals. The proposed algorithm is designed as a combination of the Gaussian mixture model and a statistical shape model. The main advantage of our algorithm is a coupled-feature of (1) robustness against outliers originating in the Gaussian mixture model with explicit outlier modeling and a built-in annealing scheme, (2) the effective reduction of the search space by incorporating prior shape information and a smooth displacement field, and (3) the simultaneous optimization of scale, translation, rotation, and shape deformation to register two point sets. Also, our approach is scalable to large point sets as the computational cost can be reduced to linear. The effectiveness of the proposed algorithm was tested through comparisons with existing point set registration algorithms, for which high quality implementations are available.

2 Methods

In this section, we review the statistical shape model based on the principal component analysis and then introduce a point set registration technique based on the Gaussian mixture model (GMM) [11, 12]. Finally, we propose a novel registration algorithm for fitting the statistical shape model combined with GMM.

2.1 Statistical shape model

We begin with definitions of a landmark and a shape, required to define a statistical shape model. To obtain shape statistics from multiple geometric objects, it is essential to define correspondent points across them. These points of correspondence are called *landmarks*. A *shape* is typically defined as a set of landmarks for one of the geometric objects with scale, rotation, and translation effects removed [30, 34]. Note here that a point set and a shape are distinguished from each other in that (1) shapes are composed of the same number of points whereas the number of points in a point set is generally different from those in other point sets, and (2) points in shapes are correspondent across all shapes, whereas points in multiple point sets are not correspondent. Statistical shape models are constructed from training shapes, i.e., multiple point sets with point-by-point correspondence.

Definition of a statistical shape model

The statistical shape model (SSM) is a representation of a geometrical shape and its statistical variations in an object. Since definitions of SSM diverge according to the aim of the application or the method of construction

[31], we introduce a definition based on the principal component analysis (PCA) [28, 29, 30], that can adequately describe the proposed algorithm. Suppose a shape is composed of M landmarks (v_1, \dots, v_M) , each of which lies in a D -dimensional space. Then, the shape is represented as a vector $\mathbf{v} = (v_1^T, \dots, v_M^T)^T \in \mathbb{R}^{MD}$. The PCA-based statistical shape model is defined as follows

$$\mathbf{v} = \mathbf{u} + \sum_{k=1}^K z_k \mathbf{h}_k + \mathbf{w}, \quad (1)$$

where $\mathbf{v} = (v_1^T, \dots, v_M^T)^T \in \mathbb{R}^{MD}$ is the mean shape, $\mathbf{h}_k \in \mathbb{R}^{MD}$ is the k th leading shape variation, $z_k \in \mathbb{R}$ is the k th weight corresponding to the k th shape variation, K is the number of shape variations, and $\mathbf{w} \in \mathbb{R}^{MD}$ is a residual vector. To reduce information sharing in shape variations to the maximum extent, $\mathbf{h}_1, \dots, \mathbf{h}_K$ are usually assumed to satisfy the orthonormality condition $\mathbf{h}_i^T \mathbf{h}_j = \delta_{ij}$ where δ_{ij} is Kronecker's delta.

Estimation of shape variations from training data

Mean shape \mathbf{u} and shape variations $\mathbf{h}_1, \dots, \mathbf{h}_K$ are unknown, and should be estimated from multiple shapes $\mathbf{v}_1, \dots, \mathbf{v}_B$, i.e., training data. The mean shape \mathbf{u} is simply estimated as the average of sample shapes. Suppose $\mathbf{C} \in \mathbb{R}^{MD \times MD}$ is a shape covariance matrix defined as

$$\mathbf{C} = \frac{1}{B-1} \sum_{j=1}^B (\mathbf{v}_j - \bar{\mathbf{v}})(\mathbf{v}_j - \bar{\mathbf{v}})^T, \quad (2)$$

where $\bar{\mathbf{v}}$ is the sample average of shapes $\mathbf{v}_1, \dots, \mathbf{v}_B$. The shape covariance matrix \mathbf{C} represents statistical dependencies for landmark displacements. The k th shape variation can be estimated as the k th eigenvector of \mathbf{C} corresponding to the k th largest eigenvalue. We note that the shape covariance matrix is dependent on rotations of shapes $\mathbf{v}_1, \dots, \mathbf{v}_B$. On the contrary, coherent moves of landmarks caused by the rotation of a whole shape cannot be represented as their covariance if the rotation angle is relatively large. Therefore, effects of rigid transformations must be eliminated from the training shapes $\mathbf{v}_1, \dots, \mathbf{v}_B$ in computing the shape covariance matrix \mathbf{C} .

2.2 Gaussian mixture model for point set registration

We summarize the Gaussian mixture modeling approach for solving point set registration problems proposed by Myronenko et al. [12], since this approach is the basis for the proposed algorithm. They defined a registration problem of two point sets as a problem of probabilistic density estimation, where one point set is composed of centroids for a Gaussian mixture model (GMM), and the other consists of samples generated from the GMM. We here refer to a point set to be deformed as a *floating* point set and the other point set that remains fixed as a *target* point set. We also refer a point irrelevant to the true object geometry as an *outlier* and the one that comprises the true object geometry as an *inlier*. Suppose $x_n \in \mathbb{R}^D$ and $y_m \in \mathbb{R}^D$ are the n th point in a target point set $X = \{x_1, \dots, x_N\}$ and the m th point in a floating point set $Y = \{y_1, \dots, y_M\}$, respectively. The probabilistic model for registering the two point sets X and Y is designed as a mixture model for generating target point x_n in the four-step procedure: (1) a label is selected as either of an outlier or an inlier based on the Bernoulli distribution with outlier probability ω , (2) if the label is inlier, a point is selected from the floating point set $Y = \{y_1, \dots, y_M\}$ with equal probability $p(m) = 1/M$, (3) the selected point y_m is moved by the transformation model \mathcal{T} , and (4) target point x_n is generated by the Gaussian distribution whose center is the moved point. More formally, the mixture model is defined as follows:

$$p(x_n; \Theta) = \omega \cdot p_{\text{outlier}}(x_n) + (1 - \omega) \cdot \sum_{m=1}^M p(m) p(x_n | m; \Theta), \quad (3)$$

where Θ is a set of parameters of the mixture model, and $p_{\text{outlier}}(x_n)$ is a distribution of outliers. The prior distribution of inliers is defined as $p(m) = 1/M$. The inlier distribution $p(x_n | m; \Theta)$ for $m = 1, \dots, M$ is defined as a Gaussian distribution

$$p(x_n | m; \Theta) = \frac{1}{(2\pi\sigma^2)^{D/2}} \exp\left(-\frac{\|x_n - \mathcal{T}(y_m; \theta)\|^2}{2\sigma^2}\right), \quad (4)$$

where σ^2 is the variance of the Gaussian distribution, $\mathcal{T}(y_m; \theta)$ is a transformation model for floating point y_m with a set of parameters θ , and $\Theta = (\theta, \sigma^2)$ is a set of parameters of the GMM. Based on the construction of GMM, the point set registration problem is defined as the minimization of the negative log-likelihood function with a regularization term as follows:

$$\hat{\Theta} = \operatorname{argmin}_{\Theta} \left\{ - \sum_{n=1}^N \log p(x_n; \Theta) + \gamma \mathcal{R}(\mathcal{T}) \right\}, \quad (5)$$

where $\mathcal{R}(\mathcal{T})$ is the regularizer in the motion coherence theory [35] and $\gamma > 0$ is a parameter that controls the degree of the smoothness for the displacement field. Since the analytic solution for Eq. (5) is not available, the EM algorithm is used to search for a local minimum of the function. The EM algorithm iteratively improves a solution by updating the upper bound of the negative log-likelihood function, called the Q -function. Given a current estimate $\bar{\Theta} = (\bar{\sigma}^2, \bar{\theta})$, the Q -function for the GMM is derived as

$$Q(\Theta, \bar{\Theta}) = \frac{N_P D}{2} \log \sigma^2 + \frac{1}{2\sigma^2} \sum_{n=1}^N \sum_{m=1}^M p(m|x_n, \bar{\Theta}) \|x_n - \mathcal{T}(y_m; \theta)\|^2 + \gamma \mathcal{R}(\mathcal{T}) \quad (6)$$

where $N_P = \sum_{n=1}^N \sum_{m=1}^M p(m|x_n, \bar{\Theta}) \leq N$ is the effective number of matching points, and $p(m|x_n, \bar{\Theta})$ denotes the posterior probability that floating point y_m is correspondent to target point x_n under the current estimate $\bar{\Theta}$. The posterior probability $p(m|x_n; \bar{\Theta})$ can be calculated as

$$p(m|x_n; \bar{\Theta}) = \frac{p(x_n|m; \bar{\Theta})}{\omega p_{\text{outlier}}(x_n) + (1 - \omega) \frac{1}{M} \sum_{m'=1}^M p(x_n|m'; \bar{\Theta})}. \quad (7)$$

Based on the theory of the EM algorithm, a solution of the point set registration problem is obtained by iterating the following procedure: (i) updating the posterior probability $p(m|x_n; \bar{\Theta})$, (ii) finding Θ^* which minimizes the Q -function for Θ given the parameter set $\bar{\Theta}$, and (iii) replacing the given parameter set $\bar{\Theta}$ with the minimizer Θ^* of the Q -function. This procedure is iterated until a suitable convergence criterion is satisfied. We note that the residual variance σ^2 corresponds to temperature T used in the annealing step for thin plate spline robust point matching (TPS-RPM) [6]. From Eq. (4) and Eq. (7), we see that matching between point sets tend to be more random if σ^2 is large and less random if it is small. To avoid local minima, TPS-RPM requires some heuristics to reduce the temperature T during optimization. On the contrary, σ^2 can be estimated during optimization, and thereby do not require any heuristics for decreasing σ^2 .

We also note that the outlier distribution $p_{\text{outlier}}(x)$ is somewhat of arbitrary choice according to applications. In this work, we use D -dimensional uniform distribution defined as $p_{\text{outlier}}(x_n) = 1/S$ where S is the volume of the region in which outliers can be generated. The volume S is of course unknown and we estimate S based on the minimum-variance unbiased estimator of the D -dimensional uniform distribution that is calculated from the target point set X .

2.3 Dependent landmark drift

We propose a novel algorithm, which we call dependent landmark drift (DLD), for registering the mean shape and a point set. The algorithm uses the same GMM framework as the CPD algorithm. The merits of using a GMM, such as in the explicit modeling of outliers and a built-in annealing scheme, are thereby inherited by the proposed algorithm. The main difference between CPD and DLD is in the definition of transformation models for a floating point set: the transformation model of CPD is based on the motion coherence, i.e., moving points under a smooth displacement field, whereas that of DLD is a combination of a statistical shape model, a rigid transformation, and the motion coherence.

Statistical shape model as a transformation model

We first describe that statistical shape models can be utilized as a transformation model for GMM-based point set registration. Suppose $h_{mk} \in \mathbb{R}^D$ is a subvector of the k th shape variation \mathbf{h}_k , corresponding to the m th landmark $u_m \in \mathbb{R}^D$ in the mean shape $\mathbf{u} \in \mathbb{R}^{MD}$. We also denote K shape variation vectors corresponding to the m th landmark by a D -by- K matrix $H_m = (h_{m1}, \dots, h_{mK}) \in \mathbb{R}^{D \times K}$. Then, the statistical shape model (1) is denoted by a point-by-point transformation model

$$v_m = u_m + H_m z + w_m, \quad (8)$$

Algorithm 1: Dependent Landmark Drift

· Input: $X = (x_1, \dots, x_N)^T$, $\mathbf{u} = (u_1^T, \dots, u_M^T)^T$, $\mathbf{H} = (H_1^T, \dots, H_M^T)^T$, Λ_K , $\omega \in (0, 1)$, $\gamma > 0$.

· Output: $Y = (y_1, \dots, y_M)^T$.

· Initialization:

$$Y = U, \quad S = \text{volume}(X), \quad \sigma^2 = \frac{1}{NMD} \sum_{n=1}^N \sum_{m=1}^M \|x_n - y_m\|^2.$$

· EM optimization: repeat until convergence.

- E-step: compute p_{mn} , $p_{m\cdot}$, $p_{\cdot n}$ for each m and n .

$$p_{mn} = \frac{\exp\left(-\frac{1}{2\sigma^2}\|x_n - y_m\|^2\right)}{\sum_{m=1}^M \exp\left(-\frac{1}{2\sigma^2}\|x_n - y_m\|^2\right) + (2\pi\sigma^2)^{D/2} \frac{\omega}{1-\omega} \frac{M}{V}},$$

$$p_{m\cdot} = \sum_{n=1}^N p_{mn}, \quad p_{\cdot n} = \sum_{m=1}^M p_{mn}, \quad N_P = \sum_{n=1}^N \sum_{m=1}^M p_{mn},$$

- M-step: update z , s , R , d , Y , \mathbf{u} , \mathbf{H} and σ^2 .

(a) Update shape parameters z , translation vector d , and shape Y .

$$x_P = \frac{1}{N_P} \sum_{n=1}^N p_{\cdot n} x_n, \quad u_P = \frac{1}{N_P} \sum_{m=1}^M p_{m\cdot} u_m, \quad H_P = \frac{1}{N_P} \sum_{m=1}^M p_{m\cdot} H_m,$$

$$z = \left\{ \sum_{m=1}^M p_{m\cdot} H_m^T H_m - N_P H_P^T H_P + \gamma \Lambda_K^{-1} \right\}^{-1} \left\{ \sum_{n=1}^N \sum_{m=1}^M p_{mn} H_m^T (x_n - u_m) - N_P H_P^T (x_P - u_P) \right\},$$

$$d = x_P - u_P - H_P z, \quad y_m = u_m + H_m z + d, \quad \text{for all } m = 1, \dots, M, \quad y_P = \frac{1}{N_P} \sum_{m=1}^M p_{m\cdot} y_m.$$

(b) Update pose parameters (s, R, d) , shape model (\mathbf{u}, \mathbf{H}) , and shape Y .

$$A = \sum_{m=1}^M \sum_{n=1}^N p_{mn} (x_n - x_P)(y_m - y_P)^T, \quad \text{compute SVD of } A = \Phi L \Psi^T,$$

$$R = \Phi \text{d}(1, \dots, 1, \det(\Phi \Psi^T)) \Psi^T, \quad s = \text{tr}(A^T R) / \sum_{m=1}^M p_{m\cdot} \|y_m - y_P\|^2, \quad d = x_P - s R y_P,$$

$$u_m \leftarrow s R u_m + d, \quad H_m \leftarrow s R H_m, \quad y_m \leftarrow s R y_m + d, \quad \text{for all } m = 1, \dots, M.$$

(c) Update residual variance σ^2 .

$$\sigma^2 = \frac{1}{N_P D} \sum_{n=1}^N \sum_{m=1}^M p_{mn} \|x_n - y_m\|^2.$$

Figure 1: Registration algorithm for the mean shape \mathbf{u} and point set X . The mean shape \mathbf{u} is also denoted by the matrix notation $U = (u_1, \dots, u_M)^T$. The notation $\text{d}(\cdot)$ denotes the operation for converting a vector into a diagonal matrix, $\det(\cdot)$ denotes the determinant of a square matrix, and the symbol “ \leftarrow ” denotes the substitution.

where v_m is the m th point in shape $\mathbf{v} \in \mathbb{R}^D$, $z = (z_1, \dots, z_K) \in \mathbb{R}^K$ is a weight vector for K shape variations, and $w_m \in \mathbb{R}^D$ is a subvector of the residual vector \mathbf{w} corresponding to landmark u_m . Therefore, the statistical shape model can be used as a transformation model of a point set registration. A merit of using statistical shape models for point set registration problems is that moves of landmarks are estimated based on the *statistical dependency* of landmark displacements. We therefore call our algorithm *dependent landmark drift*.

Transformation model

We incorporate prior shape information into the transformation model. We suppose that the training phase has already finished, and the mean shape $\mathbf{u} = (u_1^T, \dots, u_M^T)^T$ and shape variations $\mathbf{H} = (\mathbf{h}_1, \dots, \mathbf{h}_K)$, also denoted by $\mathbf{H} = (H_1^T, \dots, H_M^T)^T$, have been calculated. We then define the transformation model \mathcal{T}_{DLD} as a combination of the rigid transformation and the statistical shape model encoding prior shape information as follows,

$$\mathcal{T}_{\text{DLD}}(u_m; \theta) = sR(u_m + H_m z) + d, \quad (9)$$

where $s \in \mathbb{R}$ is a scale parameter, $R \in \mathbb{R}^{D \times D}$ is a rotation matrix, and $d \in \mathbb{R}^D$ is a translation vector. We incorporated the rigid transformation into the transformation model because the effects of scale, translation, and rotation are eliminated from the statistical shape model during training. We refer to the triplet $\rho = (s, R, d)$ as *pose parameters* and z as *shape parameters*.

Definition of Q -function

We use the Gaussian mixture model, defined as Eqs. (3) and (4), as the basis of solving the point set registration problems. We suppose $\lambda_k \in \mathbb{R}$ is the k th largest eigenvalue of the covariance matrix \mathbf{C} computed from training data and $\Lambda_K \in \mathbb{R}^{K \times K}$ is the diagonal matrix defined as $\Lambda_K = \text{d}(\lambda_1, \dots, \lambda_K)$, where $\text{d}(\cdot)$ denotes the operation of converting a vector into a diagonal matrix. Replacing the transformation model \mathcal{T} in Eq. (6) by \mathcal{T}_{DLD} , we define the Q -function of the point set registration problem as

$$Q_{\text{DLD}}(\Theta, \bar{\Theta}) = \frac{N_P D}{2} \log \sigma^2 + \frac{1}{2\sigma^2} \sum_{n=1}^N \sum_{m=1}^M p_{mn} \|x_n - sR(u_m + H_m z) - d\|^2 + \gamma z^T \Lambda_K^{-1} z, \quad (10)$$

where $\Theta = (z, \rho, \sigma^2)$, $p_{mn} = p(m|x_n; \bar{\Theta})$, and $N_P = \sum_{n=1}^N \sum_{m=1}^M p_{mn}$. We used the Tikonov regularizer $z^T \Lambda_K^{-1} z$ as a regularization term to avoid searching for extreme shapes, where $\gamma > 0$ is a parameter that controls the search space of z . We note that this regularization is interpreted as a smooth displacement field because the resulting transformed shape becomes increasingly similar to the mean shape as γ increases, i.e. the neighboring points move coherently. The prior shape information in our approach is thereby a combination of the statistical shape model, the rigid transformation, and the motion coherence.

Optimization

Based on the theory of the EM algorithm, a solution to the point set registration problem is obtained by iterating the following procedure: (i) updating the posterior probability $p_{mn} = p(m|x_n; \bar{\Theta})$, (ii) finding Θ^* that minimizes the Q -function for Θ given the parameter set $\bar{\Theta}$, and (iii) replacing the given parameter set $\bar{\Theta}$ with the minimizer Θ^* of the Q -function. Since the analytic solution Θ^* is unavailable, we divide the optimization procedure (ii) into three steps:

- (a) Optimization of shape parameter z and translation vector d given (s, R, σ^2) ,
- (b) Optimization of pose parameter $\rho = (s, R, d)$ given (z, σ^2) ,
- (c) Optimization of residual variance σ^2 given (z, ρ) .

For each step, it is possible to find the exact minimizer of the Q -function given corresponding fixed parameters. For the steps (a) and (c), the exact minimizers are obtained by taking partial derivatives of Q_{DLD} , and equating them to zero. For the step (b), Q_{DLD} must be optimized under the orthonormality condition $R^T R = I_D$ as R is a rotation matrix. This constrained optimization problem can be analytically solved by using the result reported in [36]. The residual variance σ^2 can be estimated in the same manner as for the general case of the GMM-based registration, and the built-in annealing scheme in GMM is retained.

The mean shape \mathbf{u} and shape variations \mathbf{H} are updated in the step (b) after updating the scale parameter s and the rotation matrix R since \mathbf{u} and \mathbf{H} are dependent on the coordinate system in which the statistical shape model is defined. Translation vector d is updated in the both (b) and (c) of the M-step to find a better approximation of the exact minimizer Θ^* in a heuristic manner. The DLD algorithm is summarized in Figure 1.

Linear time algorithm

The bottleneck of the algorithm is the computation of p_{mn} for all $m = 1, \dots, M$ and $n = 1, \dots, N$. The computational cost of evaluating all p_{mn} is $O(MN)$ for one iteration of the EM algorithm. Fortunately, the direct evaluation of p_{mn} can be avoided and can be computed in $O(M + N)$ time through approximate computations. Suppose $P \in \mathbb{R}^{M \times N}$ is the matrix, the m nth element of which is p_{mn} . By using this matrix notation, Algorithm 1 can be replaced by Algorithm 2 shown in Figure 2. All computations related to P in Algorithm 2 are expressed as any of $P1_N$, P^T1_M , and PX . We here also suppose $K_{YX} \in \mathbb{R}^{M \times N}$ is a Gaussian affinity matrix, the m nth element of which is defined as $k_{mn} = \exp\{-\|x_n - y_m\|^2/2\sigma^2\}$. The bottleneck matrix-vector products $P1_N$, P^T1_M , and PX can be computed as follows,

$$\begin{aligned} q &= 1_N ./ (K_{YX}^T 1_M + c 1_N) \\ P^T 1_M &= 1_N - cq, \\ P 1_N &= K_{YX} q, \\ PX &= K_{YX} d(q) X, \end{aligned} \tag{11}$$

where “./” denotes element-wise division, $c = (2\pi\sigma^2)^{D/2} \frac{\omega}{1-\omega} \frac{M}{S}$ is a constant, and $d(\cdot)$ denotes the operation for converting a vector into a diagonal matrix. The bottleneck computations $P1_N$, P^T1_M , and PX are thereby reduced to the products between the Gaussian affinity matrix K_{YX} and vectors of size M and N , that is, $K_{YX}^T a$ and $K_{YX} b$ for arbitrary vectors $a \in \mathbb{R}^M$ and $b \in \mathbb{R}^N$.

These matrix-vector products $K_{YX}^T a$ and $K_{YX} b$ can be evaluated in $O(M + N)$ using approximation techniques such as the improved fast Gauss transform [37] and the Nyström method [38]. In this work, we use the Nyström method as approximation technique because of the simplicity of its implementation. Suppose that V is the set of points that is randomly chosen L times from the combined point set $Z = X \cup Y$ without replacement. The Gaussian affinity matrix K_{YX} can be approximated by the Nyström method as follows,

$$K_{YX} \approx K_{YV} K_{VV}^{-1} K_{VX}, \tag{12}$$

where $K_{YV} \in \mathbb{R}^{M \times L}$, $K_{VV} \in \mathbb{R}^{L \times L}$, and $K_{VX} \in \mathbb{R}^{L \times N}$ are the Gaussian affinity matrices between Y and V , for the subset V itself, and between V and X , respectively. If the number of sampled points L is much less than N and M , the approximation of the products $K_{YX}^T a$ or $K_{YX} b$ can be efficiently calculated by evaluating matrix-vector products in the right-hand side of the following equations

$$\begin{aligned} K_{YX}^T a &\approx K_{VX}^T K_{VV}^{-1} K_{YV}^T a, \\ K_{YX} b &\approx K_{YV} K_{VV}^{-1} K_{VX} b, \end{aligned} \tag{13}$$

from right to left. The computational costs of evaluating the right-hand-side equations are $O(DL(M + N) + L^3 + DL^2)$, i.e., in linear time if we assume that L and D are constants. One issue of using the Nyström method is the trade-off between speed and accuracy; setting L to a small value leads to a fast but less accurate computations. We therefore directly evaluate Eqs. (11) if the residual variance σ is sufficiently small and they can be efficiently computed by evaluating affinity values among only neighbor points using the KD tree search.

The computations of the other terms in Algorithm 2 can be evaluated in $O(M + N)$ time. The product $P\tilde{X}$ in Algorithm 2 is computed in $O(M + N)$ time because $P\tilde{X} = PX - (P1_N)x_P^T$. We note that direct evaluations of diagonal matrices such as $d(q)$, $d(P1_N)$, $d(P^T1_M)$, \mathbf{P} and I_M , which can also be a bottleneck, but are avoided as the computations of off-diagonal elements can be ignored. Therefore, the computational cost of one iteration of the EM algorithm is proportional to $M + N$. We also note that the initialization step requires $O(M + N)$ computations since $\sum_{n=1}^N \sum_{m=1}^M x_n^T y_m = 1_N^T X Y^T 1_M$ can be computed by evaluating matrix-vector products of the right-hand side equation from left to right.

Algorithm 2: Dependent Landmark Drift (Linear time algorithm)

· Input: $X = (x_1, \dots, x_N)^T$, $\mathbf{u} = (u_1^T, \dots, u_M^T)^T$, $\mathbf{H} = (H_1^T, \dots, H_M^T)^T$, Λ_K , $\omega \in (0, 1)$, $\gamma > 0$.

· Output: $Y = (y_1, \dots, y_M)^T$.

· Initialization:

$$Y = U, \quad S = \text{volume}(X), \quad \sigma^2 = \frac{1}{NMD} \{M \text{tr}(X^T X) - 2(1_M^T Y X^T 1_N) + N \text{tr}(Y^T Y)\}.$$

· EM optimization: repeat until convergence.

- E-step: calculate $P1_N$, $P^T 1_M$, and PX using the Nyström method.

- M-step: update $z, s, R, d, \mathbf{u}, \mathbf{H}, Y$ and σ^2 .

(a) Update shape parameters z , translation vector d , and shape Y .

$$\begin{aligned} N_P &= 1_M^T P 1_N, \quad \mathbf{P} = \text{d}((P 1_N) \otimes 1_D), \quad \mathbf{x}_P = v(PX), \quad \mathbf{u}_P = \mathbf{P}\mathbf{u}, \\ H_P &= N_P^{-1} (1_M^T \otimes I_D) \mathbf{P}\mathbf{H}, \quad x_P = N_P^{-1} X^T P^T 1_M, \quad u_P = N_P^{-1} U^T P 1_N, \\ z &= \{\mathbf{H}^T \mathbf{P}\mathbf{H} - N_P H_P^T H_P + \gamma \Lambda_K^{-1}\}^{-1} \{\mathbf{H}^T (\mathbf{x}_P - \mathbf{u}_P) - N_P H_P^T (x_P - u_P)\}, \\ d &= x_P - u_P - H_P z, \quad Y = U + (H_1 z, \dots, H_M z)^T + 1_M d^T, \quad y_P = N_P^{-1} Y^T P 1_N. \end{aligned}$$

(b) Update pose parameters (s, R, d) , shape model (\mathbf{u}, \mathbf{H}) , and shape Y .

$$\begin{aligned} \tilde{X} &= X - 1_N x_P^T, \quad \tilde{Y} = Y - 1_M y_P^T, \quad A = (P \tilde{X})^T \tilde{Y}, \quad \text{compute SVD of } A = \Phi L \Psi^T, \\ R &= \Phi \text{d}(1, \dots, 1, \det(\Phi \Psi^T)) \Psi^T, \quad s = \text{tr}(A^T R) / \text{tr}(\tilde{Y}^T \text{d}(P 1_N) \tilde{Y}), \quad d = x_P - s R y_P, \\ \mathbf{u} &\leftarrow s(I_M \otimes R)\mathbf{u} + 1_M \otimes d, \quad \mathbf{H} \leftarrow s(I_M \otimes R)\mathbf{H}, \quad Y \leftarrow s Y R^T + 1_M d^T. \end{aligned}$$

(c) Update residual variance σ^2 .

$$\sigma^2 = \frac{1}{N_P D} \left\{ \text{tr}(X^T \text{d}(P^T 1_M) X) - 2 \text{tr}(Y^T P X) + \text{tr}(Y^T \text{d}(P 1_N) Y) \right\}.$$

Figure 2: Linear time algorithm for registering mean shape \mathbf{u} and point set X . The mean shape \mathbf{u} is also denoted by the matrix notation $U = (u_1, \dots, u_M)^T$. The notation $\text{d}(\cdot)$ denotes the operation for converting a vector into a diagonal matrix, $\det(\cdot)$ denotes the determinant of a square matrix, and $v(\cdot)$ denotes the operation for converting a matrix into a vector in the row-major order. Also, 1_M and 1_N denote column vectors of all 1s of size M and N , respectively. The identity matrices of size M and D is denoted by I_M and I_D . The symbols “ \leftarrow ” and \otimes denote the substitution and the Kronecker product, respectively.

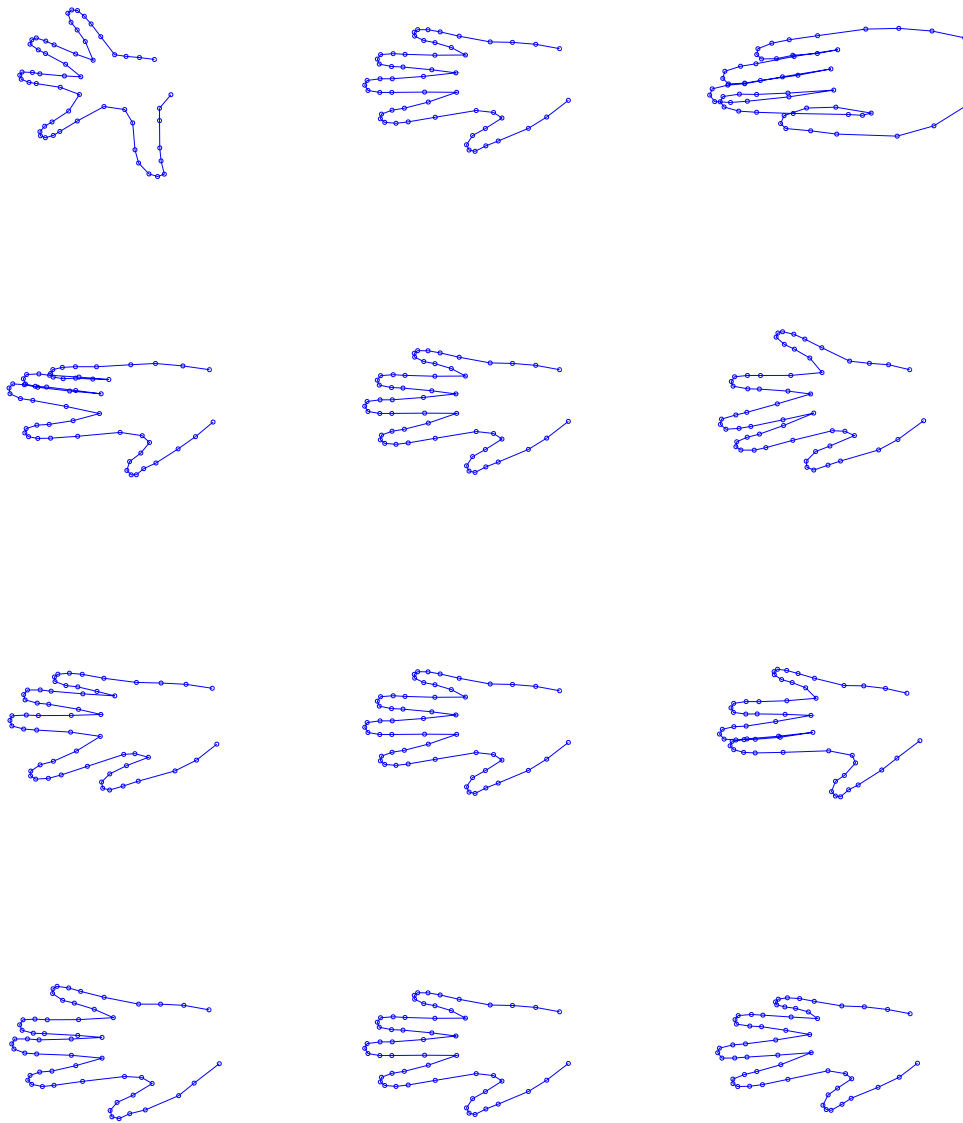


Figure 3: Mean shape deformation extracted from the IMM hand dataset. The first, the second, the third, and the fourth principal modes are shown in each row. The middle column shows the mean shape, whereas deformed mean shapes corresponding to ± 3 standard deviation are shown in the left and right columns, respectively.

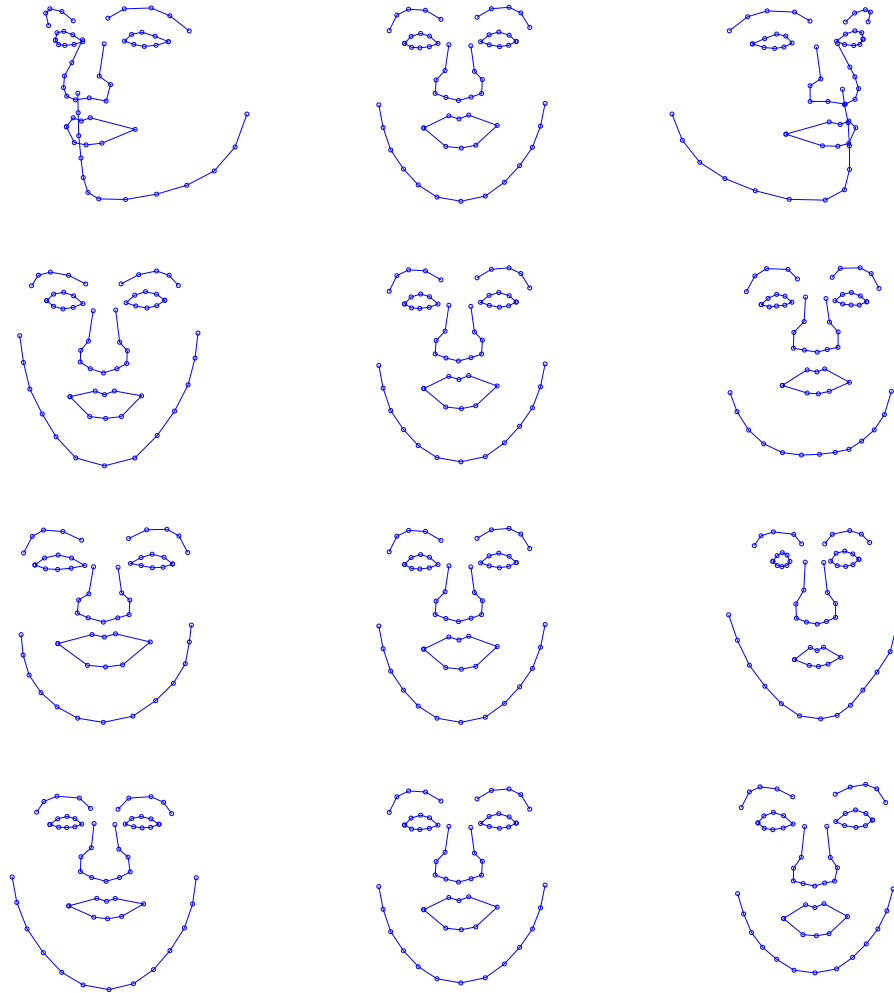


Figure 4: Mean shape deformation extracted from the IMM face dataset. The first, the second, the third, and the fourth principal modes are shown in each row. The middle column shows the mean shape, whereas deformed mean shapes corresponding to ± 3 standard deviation are shown in the left and right columns, respectively.

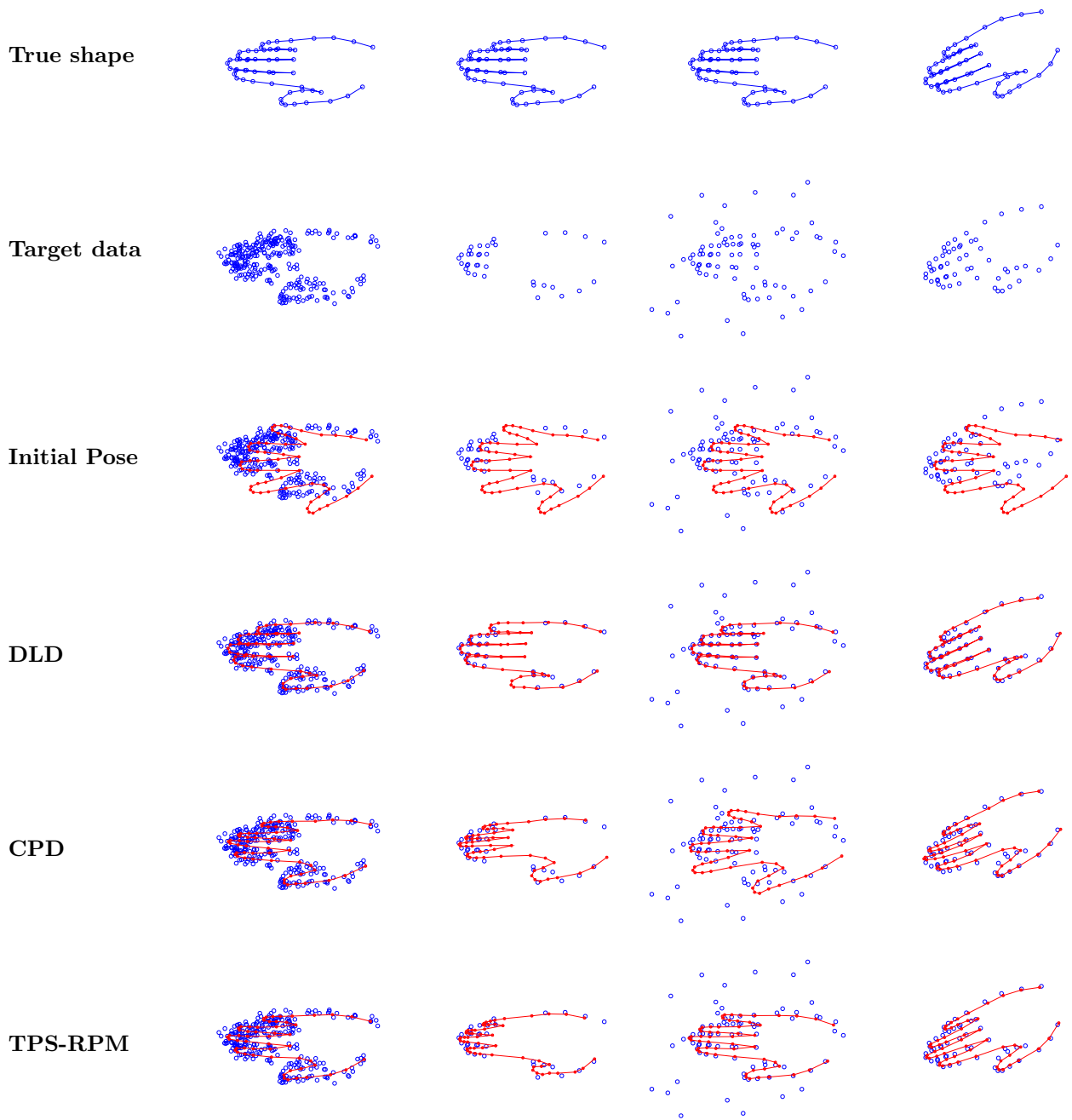


Figure 5: Applications of DLD, CPD, and TPS-RPM to hand No.6 with four types of modification: (1) replication of points with dispersion, (2) deletion of points, (3) addition of outliers, and (4) rotation of the whole shape.

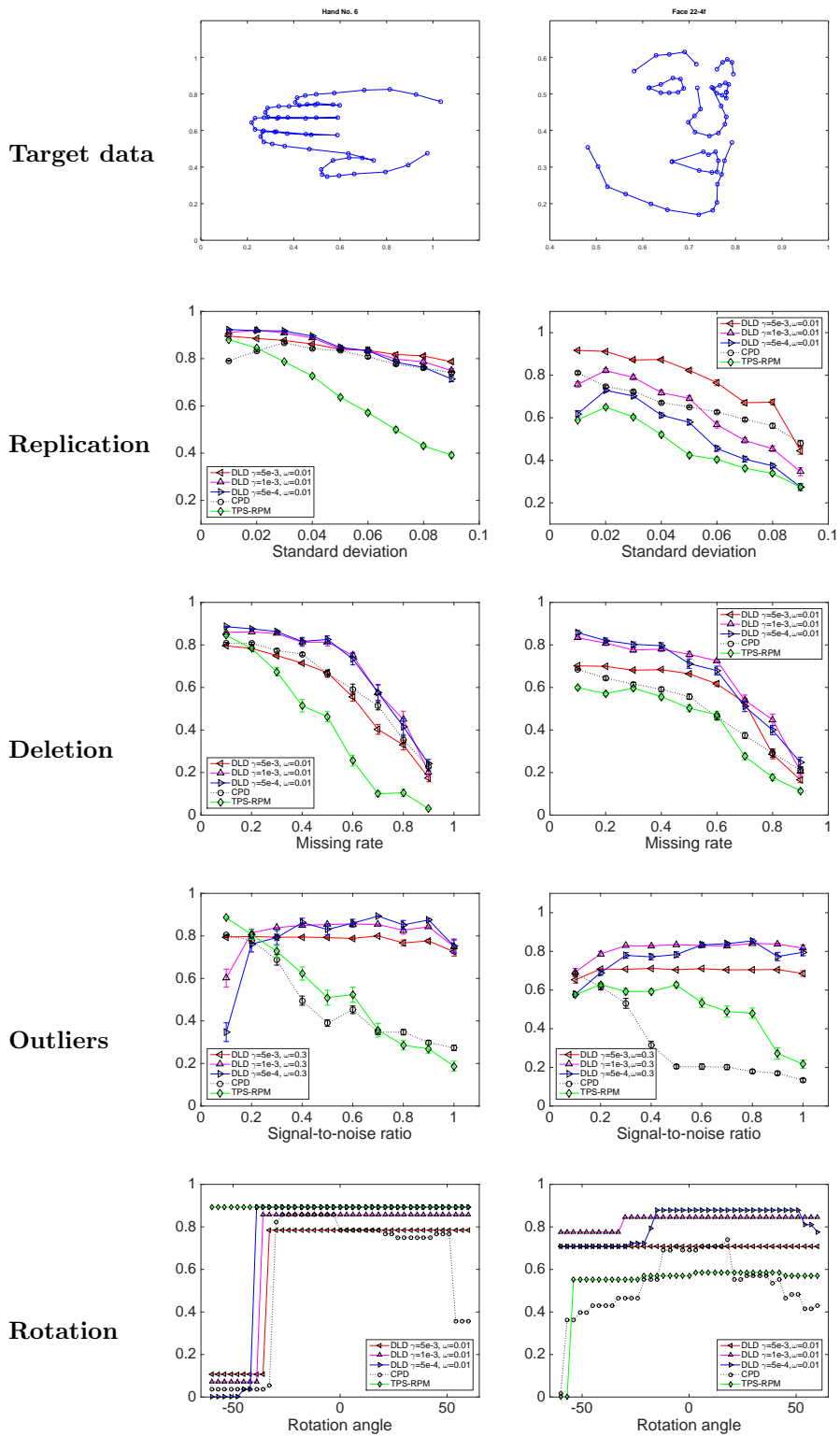


Figure 6: Comparisons of registration performance among DLD, CPD, and TPS-RPM using hand No. 6 in the IMM hand dataset (left), and face 22-4f in the IMM face dataset (right) with four types of modification (1) replication of points with dispersion, (2) deletion of points, (3) addition of outliers, and (4) rotation of the whole shape.

3 Experiments

In this section, we report the registration performance of the proposed algorithm through experimental comparisons with existing point set registration algorithms, CPD [12] and TPS-RPM [6], for which high quality implementations are distributed by the authors of the papers.

3.1 Datasets and training statistical shape models

We used the IMM hand dataset and IMM face dataset [17]. Each shape in the datasets was obtained from a 2D image of a human hand or a human face by manually placing 56 and 58 landmarks, respectively. That is, the points in the shapes were correspondent across all shapes for each dataset. The number of shapes in the hand dataset was 40, and the face dataset consisted of 240 shapes, i.e., six faces with different angles per person for 40 different people. As mentioned in the previous section, the effects of scale, rotation, and translation needed to be removed from the training data to learn the statistical shape model. To do so, we pre-processed the shapes in the original datasets as follows: For each dataset, we first calculated the mean shape as the sample average of all shapes. We then constructed training data by computing shapes with the best rigid alignment with the mean shape. Note that, from Result 7.1 described in [34], it is possible to find the best rigid transformation to match two shapes, i.e., two point sets with point-by-point correspondence. Figures 3 and 4 show the mean-shape deformations calculated from all 40 hands and 240 faces. Shape deformations obtained from the hand dataset can be roughly interpreted as the opening and closing of the mean hand, movements of the middle and the little fingers, the opening and closing of the index and the middle fingers, and the variation in the length of the little finger. Different shape variations were also extracted from the face dataset.

3.2 Illustrative results for IMM datasets

Figure 5 shows demonstrations of DLD, CPD [12] and TPS-RPM [6] for hand No. 6 with four types of modifications: (a) replication of target points with dispersion, (b) deletion of target points, (c) addition of outliers, and (d) rotation of the whole shape. We here used the hand No. 6 picked up from the original dataset instead of the pre-processed one to prevent the test problem from becoming too easy. The top row shows the true target shapes and the second row shows the target point sets with the four types of modifications. The red points shown in figures of the third row are the initial hand shapes, i.e., the mean shape of the hands, before optimization. The fourth, fifth, and sixth rows show the results of registrations using DLD, CPD, and TPS-RPM, respectively.

For all four target point sets, we fixed the parameters of DLD K and γ to $K = 10$ and $\gamma = 10^{-3}$. On the contrary, we used the remaining parameter $\omega = 0.01$ for (a), (b), and (d) and $\omega = 0.30$ for (c) since outliers were included in (c), but not included in (a), (b), and (d). For CPD and TPS-RPM, we used the software distributed by the authors of CPD and TPS-RPM with their default parameters. For DLD, we used 39 hand shapes as training data with target hand shape No. 6 removed. DLD yielded the best registration for all data. For all hand shapes deformed by CPD and TPS-RPM, images of all fingers except the thumb were rendered thinner than those of the true target shape, suggesting the weakness in assuming only a smooth displacement field as prior shape information: a point was forced to be displaced coherently with its neighboring points, even for a different finger.

For data (a), all methods roughly recovered the true target shape, whereas thinner fingers were observed for CPD and TPS-RPM. For data (b), DLD recovered the missing points correctly. On the other hand, CPD and TPS-RPM did not recover the missing points, and the thumb and all fingers were rendered shorter in their results than the true target shapes. This suggests a weakness in the computation of the missing regions. This weakness is originated in assuming only a smooth displacement field: floating points moved much more coherently as the target points did not exist near them. For data (c), DLD found the true target shape, whereas the deformed shapes generated by CPD and TPS-RPM were close to the mean shape rather than the true target shape. For data (d), all methods roughly recovered the true target shape, whereas thinner fingers were observed in results for CPD and TPS-RPM. DLD succeeded in recovering the true hand shape.

3.3 Comparison of registration performance

To evaluate the registration performances of DLD more precisely, we compared DLD, CPD, and TPS-RPM using the same IMM hand dataset and the IMM face dataset under various conditions. As the true target

shapes to be estimated, we used hand No. 6 and face 22-4f shown in the first row of Figure 6, which were clearly different from the mean shapes shown in the middle column of Figure 3 and 4, respectively. For the IMM hand dataset, we used 39 hand shapes with hand No. 6 removed from all 40 shapes as a set of training data for DLD, whereas 234 face shapes, with all six faces of human No. 22 removed, were used as the other set of training data for DLD.

Generating validation datasets

As in the experiment in the previous subsection, we generated the four types of target data for the hand No.6: (a) 20-time replication of target points with dispersion, (b) random deletion of target points, (c) addition of outliers that follows uniform distributions, and (d) rotation of the whole shape. In generating the four types of target data, we changed the parameters of data generation: (a) standard deviation of the Gaussian distribution for replicating target points, (b) missing rate, (c) signal-to-noise ratio, and (d) rotation angle. To repeat the experiments and reduce the influence of randomness on registration performance, we generated target point sets 20 times for (a), (b), and (c) in the same setting. For (d), a single set of target points was generated for each rotation angle, since there is no randomness in the case of rotation.

Definition of registration accuracy

DLD, CPD, and TPS-RPM were applied to each target data item, and the registration accuracy was calculated for each. For target data (a), (b), and (c), the average and standard errors in the registration accuracy were calculated. Registration accuracy was defined as the rate of correct matching between a true target shape and a deformed mean shape following registration. More formally, it was defined as follows

$$\text{Accuracy} = \frac{\text{\#points with correct matching}}{\text{\#points in the mean shape}}.$$

Point-by-point correspondence to compute registration accuracy was estimated using the nearest-neighbor matching between the deformed mean shape and the true target shape without modifications such as deletion of points and addition of replicated points and outliers.

Choice of parameters

We used the default parameters for CPD and TPS-RPM implemented in their software. For DLD, we fixed the number of shape variations to $K = 10$ for the hand dataset and $K = 30$ for the face dataset. We set the parameter of DLD ω to 0.01 for (a), (b), and (d), whereas 0.30 for (c) since the former datasets did not include outliers and the latter included outliers. We changed the parameter of DLD γ to 5.0×10^{-3} , 1.0×10^{-3} , 5.0×10^{-4} to investigate the influence of γ on registration performance.

Results

The second row in Figure 6 shows the results of the comparison of target shapes with replicated target points. The x -axis represents the standard deviation of replicating target points while the y -axis shows registration accuracy. For the hand datasets, the registration performance of DLD was insensitive to the regularization parameter γ and DLD outperformed CPD and TPS-RPM for almost all cases. For face datasets, DLD with $\gamma = 5.0 \times 10^{-3}$ achieved the best registration performance, whereas DLD with $\gamma = 5.0 \times 10^{-4}$ were less accurate than CPD.

The results for target shapes with random missing points are shown in the third row of Figure 6. The x -axis represents the missing rate and the y -axis registration accuracy. DLDs with $\gamma = 1.0 \times 10^{-3}$ and 5×10^{-4} were the most stable for the target shapes, and it outperformed CPD and TPS-RPM in nearly all cases. On the contrary, DLD with $\gamma = 5 \times 10^{-3}$ was moderately less accurate than CPD for the hand dataset. This suggests that too large γ sometimes reduces the registration accuracy because of the large bias originating in the prior shape information.

The fourth row in Figure 6 shows the results for target shapes with outliers following a 2D uniform distribution with $x_1 \in [0.0, 1.2]$ and $x_2 \in [0.0, 1.2]$ for the hand dataset and that with $x_1 \in [0.2, 1.0]$ and $x_2 \in [0.0, 0.8]$ for the face dataset. The x -axis of each figure represents the signal-to-noise ratio and the y -axis represents registration accuracy. DLD achieved the best registration performance for both datasets in nearly all cases, showing its robustness against outliers. In the case that the signal-to-noise ratio was 0.1, DLD was less accurate

than CPD and TPS-RPM. This suggests that inappropriate choice of noise probability ω reduces registration accuracy.

The fifth row in Figure 6 shows the results for rotated target shapes. The x -axis and the y -axis represent the rotation angle and registration accuracy, respectively. For the hand dataset, the registration accuracy of TPS-RPM was considerably stable and was unaffected by the rotation angles, at least in the range $[-\pi/3, \pi/3]$. For the face dataset, DLD achieved the best performance in nearly all cases, suggesting its robustness to the rotation.

4 Conclusion

Many existing algorithms for solving point set registration problems employ the assumption of a smooth displacement field, that is, the local geometry of the point set is preserved. Because of this assumption, registration problems are elegantly solved by these algorithms in various cases. This means that the registration performance can be improved using prior shape information instead of sacrificing the applicability of the algorithms. In this paper, we proposed a novel point set registration algorithm based on a Gaussian mixture model with explicit outlier modeling. We used a PCA-based statistical shape model to encode prior shape information, which was combined with the assumption of a smooth displacement field. The proposed algorithm works well if the target point set is rotated as pose parameters corresponding to a rigid transformation are simultaneously estimated in addition to shape deformation. Our algorithm is also scalable to large point sets because of the existence of a linear-time algorithm. To evaluate the registration performance of the proposed algorithm, we compared it with CPD and TPS-RPM using the IMM hand dataset and the IMM face dataset with four types of modifications: replication of target points with dispersion, random deletion of target points, addition of outliers, and rotation of the entire shape. The proposed algorithm outperformed CPD and TPS-RPM in almost all cases, showing its effectiveness for various types of point set registration problems.

Conflict of Interest

None declared.

References

- [1] L. G. Brown, A survey of image registration techniques, *ACM Comput. Surv.* 24 (4) (1992) 325–376.
- [2] P. Besl, N. McKay, A method for registration of 3-D shapes, *IEEE Trans. Pattern Anal. Mach. Intell.* 14 (2) (1992) 239–256.
- [3] S. Rusinkiewicz, M. Levoy, Efficient variants of the ICP algorithm, in: *Proc. Third Int. Conf. 3-D Digit. Imaging Model.*, IEEE Comput. Soc, 2001, pp. 145–152.
- [4] A. W. Fitzgibbon, Robust registration of 2D and 3D point sets, *Image Vis. Comput.* 21 (13-14) (2003) 1145–1153.
- [5] A. Makadia, A. Patterson, K. Daniilidis, Fully Automatic Registration of 3D Point Clouds, in: *Proc. IEEE Conf. Comput. Vis. Pattern Recognit.*, IEEE Comput. Soc, 2006, pp. 1297–1304.
- [6] H. Chui, A. Rangarajan, A feature registration framework using mixture models, in: *Proc. IEEE Work. Math. Methods Biomed. Image Anal.*, IEEE Comput. Soc, 2000, pp. 190–197.
- [7] H. Chui, A. Rangarajan, A new point matching algorithm for non-rigid registration, *Comput. Vis. Image Underst.* 89 (2-3) (2003) 114–141.
- [8] B. Jian, B. C. Vemuri, Robust point set registration using Gaussian mixture models, *IEEE Trans. Pattern Anal. Mach. Intell.* 33 (8) (2011) 1633–1645.
- [9] J. Chen, J. Ma, C. Yang, L. Ma, S. Zheng, Non-rigid point set registration via coherent spatial mapping, *Signal Processing* 106 (2015) 62–72.

- [10] Y. Yang, S. H. Ong, K. W. C. Foong, A robust global and local mixture distance based non-rigid point set registration, *Pattern Recognit.* 48 (1) (2015) 156–173.
- [11] A. Myronenko, X. Song, M. Á. Carreira-Perpiñán, Non-rigid point set registration: Coherent Point Drift, in: *Proc. Adv. Neural Inf. Process. Syst.* 19, MIT press, 2006, pp. 1009–1016.
- [12] A. Myronenko, X. Song, Point set registration: Coherent point drift, *IEEE Trans. Pattern Anal. Mach. Intell.* 32 (12) (2010) 2262–2275.
- [13] J. Ma, W. Qiu, J. Zhao, Y. Ma, A. L. Yuille, Z. Tu, Robust L2E estimation of transformation for non-rigid registration, *IEEE Trans. Signal Process.* 63 (5) (2015) 1115–1129.
- [14] J. Ma, J. Zhao, A. L. Yuille, Non-rigid point set registration by preserving global and Local Structures, *IEEE Trans. Image Process.* 25 (1) (2016) 53–64.
- [15] Z. Zhang, Iterative point matching for registration of free-form curves and surfaces, *Int. J. Comput. Vis.* 13 (2) (1994) 119–152.
- [16] S. Granger, X. Pennec, Multi-scale EM-ICP: A fast and robust approach for surface registration, in: *Proc. 4th Eur. Conf. Comput. Vis.*, Springer-Verlag, 2002, pp. 418–432.
- [17] C. Stewart, Chia-Ling Tsai, B. Roysam, The dual-bootstrap iterative closest point algorithm with application to retinal image registration, *IEEE Trans. Med. Imaging* 22 (11) (2003) 1379–1394.
- [18] A. Rangarajan, H. Chui, F. L. Bookstein, The Softassign Procrustes Matching Algorithm, *Lect. Notes Comput. Sci.* 1230 (1997) 29–42.
- [19] D. Chetverikov, D. Stepanov, P. Krsek, Robust Euclidean alignment of 3D point sets: The trimmed iterative closest point algorithm, *Image Vis. Comput.* 23 (3) (2005) 299–309.
- [20] Y. Tsin, T. Kanade, A correlation-based approach to robust point set registration, in: *Proc. 6th Eur. Conf. Comput. Vis.*, (ECCV'04) Springer-Verlag, 2004, pp. 558–569.
- [21] Q.-Y. Zhou, J. Park, V. Koltun, Fast global registration, in: *Proc. 14th Eur. Conf. Comput. Vis.*, (ECCV'16) Springer-verlag, 2016.
- [22] D. Mateus, R. Horaud, D. Knossow, F. Cuzzolin, E. Boyer, Articulated shape matching using Laplacian eigenfunctions and unsupervised point registration, in: *Proc. IEEE Conf. Comput. Vis. Pattern Recognit.* 2008, IEEE Comput. Soc, 2008, pp. 1–8.
- [23] R. Horaud, F. Forbes, M. Yguel, G. Dewaele, J. Zhang, Rigid and articulated point registration with expectation conditional maximization, *IEEE Trans. Pattern Anal. Mach. Intell.* 33 (3) (2011) 587–602.
- [24] S. Ge, G. Fan, Non-rigid articulated point set registration with local structure preservation, in: *Proc. IEEE Conf. Comput. Vis. Pattern Recognit. Work. 2015*, IEEE Comput. Soc, 2015, pp. 126–133.
- [25] S. Ge, G. Fan, Non-rigid articulated point set registration for human pose estimation, in: *2015 IEEE Winter Conf. Appl. Comput. Vis.*, IEEE, 2015, pp. 94–101.
- [26] I. Kolesov, J. Lee, G. Sharp, P. Vela, A. Tannenbaum, A stochastic approach to diffeomorphic point set registration with landmark constraints, *IEEE Trans. Pattern Anal. Mach. Intell.* 38 (2) (2016) 238–251.
- [27] V. Golyanik, B. Taetz, G. Reis, D. Stricker, Extended coherent point drift algorithm with correspondence priors and optimal subsampling, in: *Proc. IEEE Winter Conf. Appl. Comput. Vis.*, IEEE, 2016, pp. 1–9.
- [28] T. Cootes, C. Taylor, D. Cooper, J. Graham, Active shape models—their training and application, *Comput. Vis. Image Underst.* 61 (1) (1995) 38–59.
- [29] T. F. Cootes, C. Taylor, Statistical models of appearance for computer vision, *Tech. Rep. Univ. Manchester* (2004) 1–124
- [30] M. B. Stegmann, D. D. Gomez, A brief introduction to statistical shape analysis (2002).

- [31] T. Heimann, H. P. Meinzer, Statistical shape models for 3D medical image segmentation: a review, *Med. Image Anal.* 13 (4) (2009) 543–563.
- [32] F. P. M. Oliveira, J. M. R. S. Tavares, Medical image registration: a review, *Comput. Methods Biomech. Biomed. Engin.* 17 (2) (2012) 73–93.
- [33] A. Sotiras, C. Davatzikos, N. Paragios, Deformable medical image registration: a survey, *IEEE Trans. Med. Imaging* 32 (7) (2013) 1153–1190.
- [34] I. L. Dryden, K. V. Mardia, *Statistical shape analysis with applications in R*, Wiley Series in Probability and Statistics, John Wiley & Sons, Ltd, Chichester, UK, 2016.
- [35] A. L. Yuille, N. M. Grzywacz, A mathematical analysis of the motion coherence theory, *Int. J. Comput. Vis.* 3 (2) (1989) 155–175.
- [36] A. Myronenko, X. Song, On the closed-form solution of the rotation matrix arising in computer vision problems (2009).
- [37] C. Yang, R. Duraiswami, N.A. Gumerov, L. Davis, Improved fast Gauss transform and efficient kernel density estimation, in: *Proc. Ninth IEEE Int. Conf. Comput. Vis.*, IEEE, 2003, pp. 664–671.
- [38] Using the Nyström method to speed up kernel machines, in: *Proc. 13th Advances in Neural Information Processing Systems*, 2000, pp. 682–688.
- [39] N. Hansen, *The CMA evolution strategy: a comparing review*, in: *Toward a New Evol. Comput.*, Vol. 102, Springer-Verlag, 2011, pp. 75–102.